

Yassir Boulaamane, Mahmoud A. A. Ibrahim, Mohammed Reda Britel and Amal Maurady*

In silico studies of natural product-like caffeine derivatives as potential MAO-B inhibitors/AA_{2A}R antagonists for the treatment of Parkinson's disease

<https://doi.org/10.1515/jib-2021-0027>

Received August 28, 2021; accepted June 24, 2022; published online September 19, 2022

Abstract: Parkinson's disease is considered the second most frequent neurodegenerative disease. It is described by the loss of dopaminergic neurons in the mid-brain. For many decades, L-DOPA has been considered as the gold standard for treating Parkinson's disease motor symptoms, however, due to the decrease of efficacy, in the long run, there is an urgent need for novel antiparkinsonian drugs. Caffeine derivatives have been reported several times for their neuroprotective properties and dual blockade of monoamine oxidase (MAO) and adenosine A_{2A} receptors (AA_{2A}R). Natural products are currently attracting more focus due to structural diversity and safety in contrast to synthetic drugs. In the present work, computational studies were conducted on natural product-like caffeine derivatives to search for novel potent candidates acting as dual MAO-B inhibitors/AA_{2A}R antagonists for Parkinson's disease. Our findings revealed two natural products among the top hits: CNP0202316 and CNP0365210 fulfill the requirements of drugs acting on the brain. The selected lead compounds were further studied using molecular dynamics simulation to assess their stability with MAO-B. Current findings might shift the interest towards natural-based compounds and could be exploited to further optimize caffeine derivatives into a successful dual-target-directed drug for managing and halting the neuronal damage in Parkinson's disease patients.

Keywords: ADMET prediction; caffeine; molecular dynamics simulation; natural products; neuroprotection; structure-based virtual screening.

1 Introduction

Neurodegenerative diseases and brain-associated diseases are major concerns among aging populations across the world [1]. Neurodegenerative diseases such as Parkinson's and Alzheimer's diseases have a multifactorial nature that is characterized by the progressive loss of neurons in the brain [2]. Parkinson's disease

*Corresponding author: Amal Maurady, Laboratory of Innovative Technologies, National School of Applied Sciences of Tangier, Abdelmalek Essaadi University, Tetouan, Morocco; and Faculty of Sciences and Techniques of Tangier, Abdelmalek Essaadi University, Tetouan, Morocco, E-mail: amaurady@uae.ac.ma. <https://orcid.org/0000-0001-9298-717X>

Yassir Boulaamane and Mohammed Reda Britel, Laboratory of Innovative Technologies, National School of Applied Sciences of Tangier, Abdelmalek Essaadi University, Tetouan, Morocco, E-mail: boulaamane.yassir@etu.uae.ac.ma (Y. Boulaamane), mbritel@uae.ac.ma (M.R. Britel). <https://orcid.org/0000-0002-2939-7772> (Y. Boulaamane). <https://orcid.org/0000-0002-9918-5767> (M.R. Britel)

Mahmoud A. A. Ibrahim, Computational Chemistry Laboratory, Chemistry Department, Faculty of Science, Minia University, Minia, 61519, Egypt, E-mail: m.ibrahim@compchem.net. <https://orcid.org/0000-0003-4819-2040>

(PD) is defined especially by the progressive loss of dopaminergic neurons in the substantia nigra pars compacta (SNpc) of the midbrain [3]. More than six million people in the world are affected today with a prevalence of 150 in every 100,000 people which is further increasing with age and affects 1% of the population over 60 years [4]. Current pharmaceutical treatments for PD include levodopa or levodopa plus dopa-decarboxylase inhibitors, dopamine agonists, and catechol-O-methyl transferase (COMT)/monoamine oxidase B (MAO-B) inhibitors [5]. Recently, other non-dopaminergic drugs have shown promising efficacy to relieve PD symptoms such as adenosine A_{2A} receptor ($AA_{2A}R$) antagonists [6].

Monoamine Oxidase (MAO) (EC 1.4.3.4) belongs to a family of flavin adenine dinucleotide (FAD)-dependent enzymes that are expressed in the outer mitochondrial membrane of neuronal cells. The MAO enzymes are responsible for the oxidative deamination of monoamine neurotransmitters such as dopamine, adrenaline, and noradrenaline in the central nervous system (CNS) [5, 7]. The MAO enzymes exist in two isoforms, MAO-A and MAO-B that share sequence similarities of 70% but differ in tissue distribution, substrate, and inhibitor preferences [5]. The development of the first MAO inhibitors was abandoned due to side effects related to the metabolism of tyramine, which causes a cardiovascular crisis [8]. However, a new class of selective MAO-B inhibitors has been proven to be efficient in treating PD symptoms. It was also shown that this new class of selective MAO-B inhibitors is devoid of tyramine-related side effects. Furthermore, the selective MAO-B inhibitors may act as neuroprotective agents by limiting the release of free radical species and hence may decrease the progression of the disease [5, 9].

MAO-A preferentially metabolizes serotonin while MAO-B preferentially deaminates 2-phenylethylamine and benzylamine. Dopamine, norepinephrine, and epinephrine are substrates of both isoforms in most animal tissues [10].

During aging, the expression of MAO-B increases in the brain and is connected with an enhanced dopamine metabolism which results in an increased reactive oxygen species (ROS) production such as hydrogen peroxide (H_2O_2) inducing oxidative damage and apoptotic signaling events [11].

Previously approved MAO-B inhibitors are selegiline and rasagiline which irreversibly inhibit MAO-B with an IC_{50} value of 6.8 and 14 nM respectively [12]. The latest approved MAO-B inhibitor is safinamide which reversibly inhibits MAO-B with an IC_{50} value of 450 nM [13]. Istradefylline, a caffeine-based inhibitor that was approved in Japan in 2013 and also approved for medical use in the United States in 2019 acts as a dual inhibitor of MAO-B and $AA_{2A}R$ [14, 15]. However, istradefylline was found to be a weak inhibitor of MAO-B ($IC_{50} = 28 \mu M$) which encourages further research on new substitutions to the caffeine core [16]. The chemical structures of MAO-B inhibitors are shown in Figure 1.

The crystal structure of MAO-A (PDB ID: 2Z5Y) has a monopartite substrate cavity of $\sim 550 \text{ \AA}^3$ volume while the crystal structure of MAO-B contains a bipartite cavity structure with an entrance cavity of $\sim 290 \text{ \AA}^3$ and a substrate cavity of $\sim 400 \text{ \AA}^3$ [17]. ILE-199 and TYR-326 separate these two cavities in MAO-B serving as

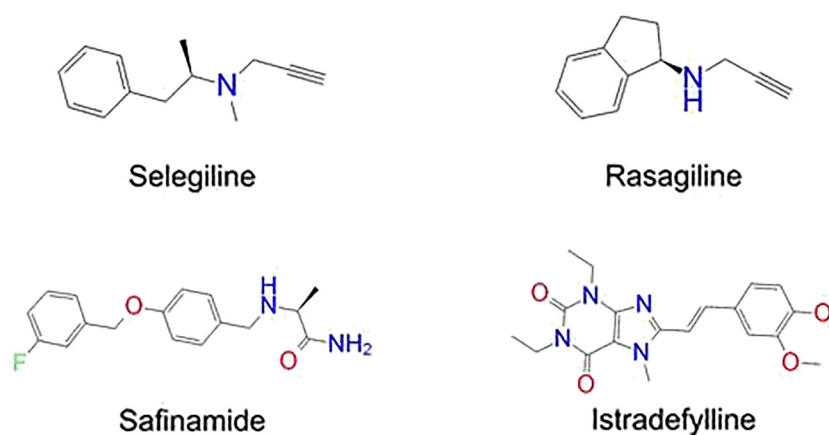


Figure 1: Chemical structures of monoamine oxidase B inhibitors.

“gating” residues and a structural determinant for substrate and inhibitor recognition by MAO-B [18, 19]. The superposition of MAO-A and MAO-B and their active site residues are shown in Figure 2.

The structural study revealed that MAO-B (PDB ID: 2V5Z) is formed by two monomers consisting of a globular domain anchored to the membrane through a C-terminal helix [20]. MAO-B active site residues that share similarities to MAO-A active site are TYR-60, LEU-164, PHE-168, GLN-206, ILE-198, ILE-316, PHE-343, TYR-398, and TYR-435. Meanwhile, the amino acids that are specific to MAO-B are located in the hydrophobic pocket which is formed by LEU-171, CYS-172, ILE-199, TYR-326 [13].

There is a great deal of literature supporting the use and efficacy of natural products (NP) in PD such as flavonoids, xanthenes, phenolic derivatives, alkaloids, and caffeine [21, 22]. These natural resources and their derivatives have been reported for their potential to selectively inhibit MAO-B and may offer a safer alternative compared to conventional drugs [23]. Furthermore, caffeine has been used in several studies as a scaffold for the design of dual MAO inhibitors/AA_{2A}R antagonists. Pretorius et al. synthesized a series

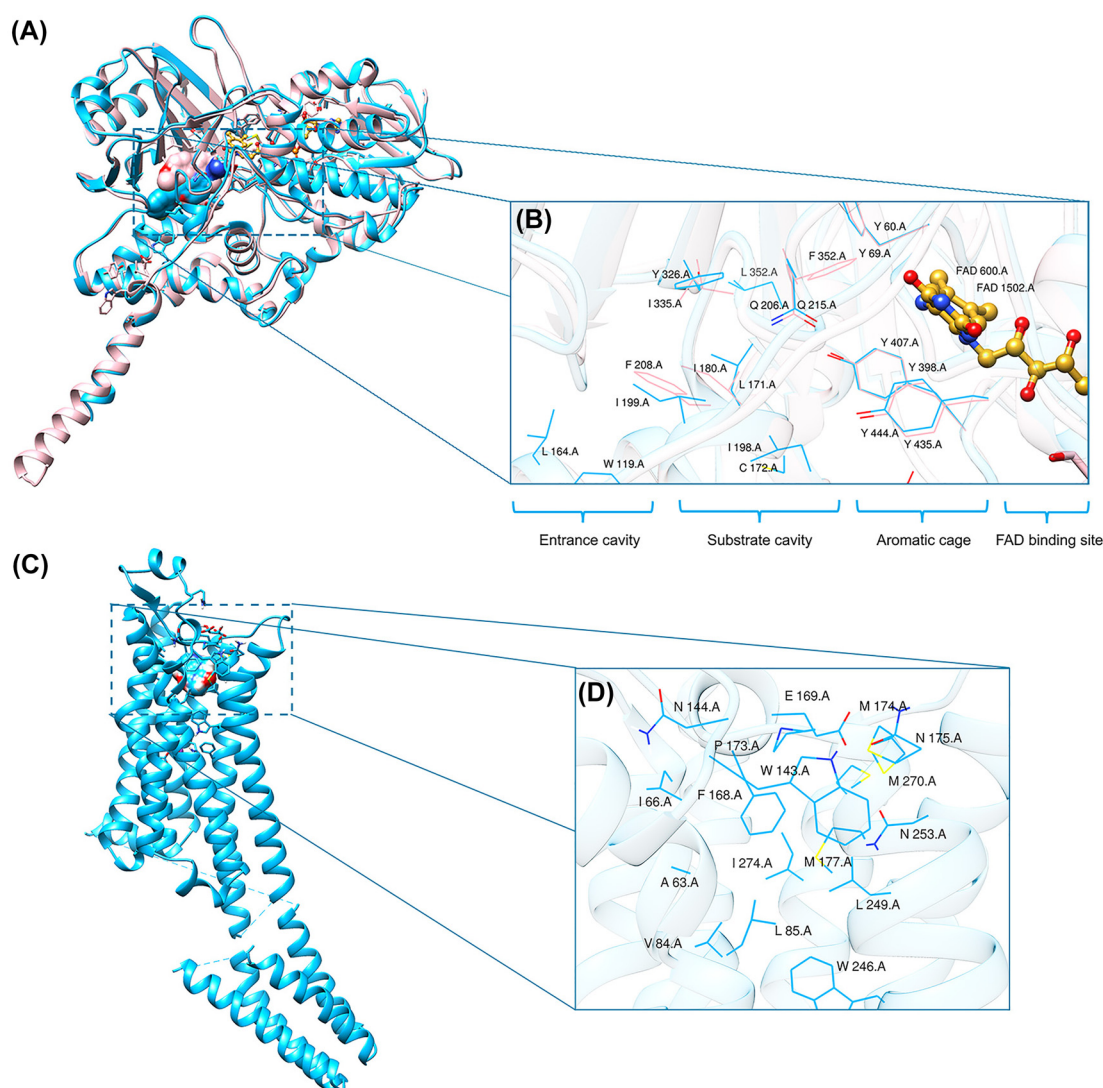


Figure 2: (A) Superposition of crystal structures of MAO-A (pink color) and MAO-B (deep sky-blue color). (B) Superposition of active site residues of MAO-A (pink color) and MAO-B (deep sky-blue color), FAD (goldenrod color) is shown in ball & stick representation. (C) Crystal structure of AA_{2A}R in complex with caffeine. (D) Active site residues of AA_{2A}R.

of C-8 substituted caffeinyl analogues and it was found that the compound bearing a 4-phenylbutadien moiety is the most potent candidate for MAO-B and AA_{2A}R [24]. On the other hand, Azam et al. explored numerous caffeine derivatives from the literature bearing multiple substitutions through molecular docking and structure-activity relationship studies, it was found that the placement of hydrophobic moieties at C8 is essential for both MAO-B inhibition and AA_{2A}R antagonism, whereas replacements occurring at C1 and C3 are optimal for AA_{2A}R but not detrimental for MAO-B [25]. Although research on caffeine is underway for decades, its naturally occurring derivatives are yet to be investigated in detail [26].

NPs and NP-based compounds are an ideal choice for scientists and researchers due to the broad-spectrum activity of NPs with their minimal or no toxic effect on human health [27]. The literature has indicated that caffeine among other NPs is a potent compound that has neuroprotective properties [28]. Considering the link between neurodegeneration and oxidative stress due to the mitochondrial imbalance and the accumulation of reactive oxygen species (ROS), MAO-B was and still is, considered a valid therapeutic target for slowing down the progression of Parkinson's disease.

In the present study, a substructure search was conducted on natural products databases to retrieve caffeine-containing natural products since it is known for its neuroprotective properties and its potency to act as an antagonist of AA_{2A}R, a validated target for PD [29]. Structure-based virtual screening was employed to evaluate the affinity of the selected natural compounds towards MAO-B and AA_{2A}R. ADMET properties were evaluated using *in silico* methods. Finally, molecular dynamics simulations were performed to study the interactions and the stability between the selected compounds and MAO-B over the simulation time.

2 Material and methods

2.1 Data sources

To retrieve all the available natural compounds based on the caffeine scaffold, we used the COCONUT database (<https://coconut.naturalproducts.net/>); the largest open-source natural products (NP) database to date containing more than 400 000 unique NP from over 50 sources [30]. The search was conducted using the Ulmann algorithm for the substructure search with the caffeine scaffold as a pharmacophore [31]. The search results revealed 144 caffeine-containing natural products. These compounds were downloaded in SDF format for further analysis.

2.2 Protein preparation and grid generation

Crystal structure of MAO-B (PDB ID: 2V5Z, resolution = 1.7 Å) in complex with safinamide and crystal structure of AA_{2A}R (PDB ID: 5M2P, resolution = 2.1 Å) in complex with caffeine were retrieved from the RCSB Protein Data Bank (<https://www.rcsb.org/>) [13]. Residues with missing atoms were fixed using the CHARMM-GUI web server [32]. Water molecules were removed since they are not involved in the ligand binding. Since MAO-B is expressed as a dimer, only one chain was kept along with the FAD cofactor for the molecular modeling studies to ease the computational cost [33]. Finally, polar hydrogens and Kollman charges were added using AutoDockTools 1.5.6 [34]. The grid box was placed near the FAD cofactor with a spacing of 1 Å. Grid dimensions were chosen large enough (24 × 24 × 24 Å in x, y, and z directions, respectively) to fit all the residues forming both cavities of the active site in the protein. The grid box was positioned in a way to cover the entire binding site and to allow larger molecules to dock properly: 53 × 155 × 27 Å for MAO-B and -21.6 × 6.1 × 17.5 for AA_{2A}R in x, y, and z directions, respectively. Lastly, the generated coordinates for the grid box were saved in a text file.

2.3 Preparation of ligands

The selected caffeine derivatives were split into multiple files, with each file containing a single ligand. The 3D conformations were generated for all the compounds, geometrical optimization was performed using Merck molecular force field (MMFF94) implemented in the Open Babel chemical toolbox [35]. The minimized ligands were then prepared for the molecular docking study using the `prepare_ligand4.py` package of AutoDockTools 1.5.6. Partial charges, atomic types, and polar hydrogens were added to all compounds and then converted to PDBQT format.

2.4 Structure-based virtual screening workflow

Structure-based virtual screening was performed using a Perl script for the automated execution of AutoDock Vina 1.1.2 [36]. The proposed methodology is detailed in Figure 3, a text file containing all the names of the prepared ligands was created to serve as a single input file for the docking screens. To facilitate the analysis of the virtual screening results, all the generated output log files were concatenated into a single output text file. All procedures were performed in respect of good practices using state-of-the-art virtual screening approaches for natural products bioprospecting as shown in Figure 4. The standard virtual screening consists mainly of target identification, selection of the chemical library, molecular docking studies, ADMET evaluation, molecular dynamics simulations, and finally experimental validation of the lead compounds [37].

2.5 Visualization and analysis

The ligands were ranked by their binding affinities. The compounds displaying a binding score of -8.0 kcal/mol or less were subject to further analysis. The conformations of the selected compounds were visualized using UCSF Chimera visualization software and superposed to the ligand of reference [38]. Discovery Studio Visualizer program was used to identify hydrogen bonds and other hydrophobic interactions [39].

2.6 *In silico* ADMET prediction

The profiling of compound pharmacokinetics is very essential in drug discovery. As of today, many online tools are available to predict the ADMET profiles of drugs based on their chemical properties [40]. *In silico* ADMET profiling can be useful to speed up the drug development process by limiting the number of compounds for experimental testing. In this study, physicochemical properties and pharmacokinetic parameters were evaluated using SwissADME online calculation toolkit (<http://www.swissadme.ch/>) [41]. Lipinski's rule of five was taken into account to assess the ability of the compounds to be active for orally administered drugs [42]. Other parameters such as water solubility, gastrointestinal absorption, and blood-brain barrier permeability were predicted. Pain-assay interference compounds (PAINS) are chemical molecules that often give false-positive results in high-throughput

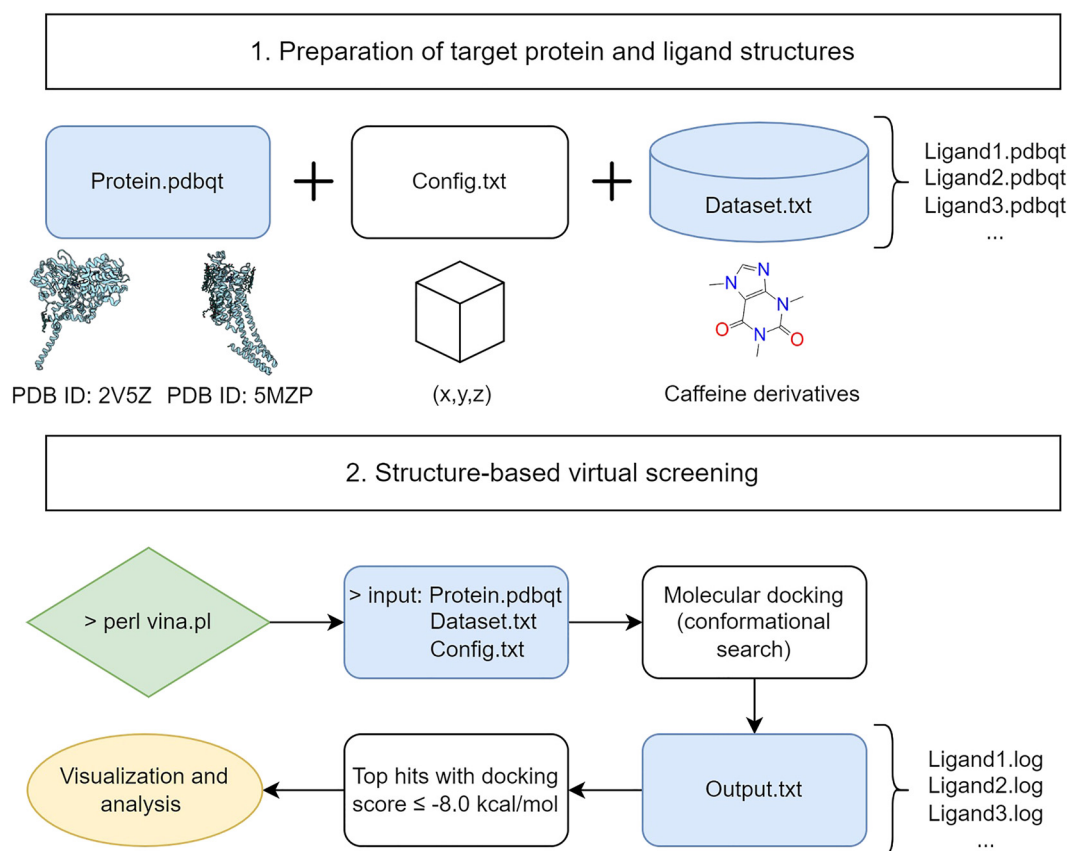


Figure 3: Proposed workflow for structure-based virtual screening using AutoDock Vina.

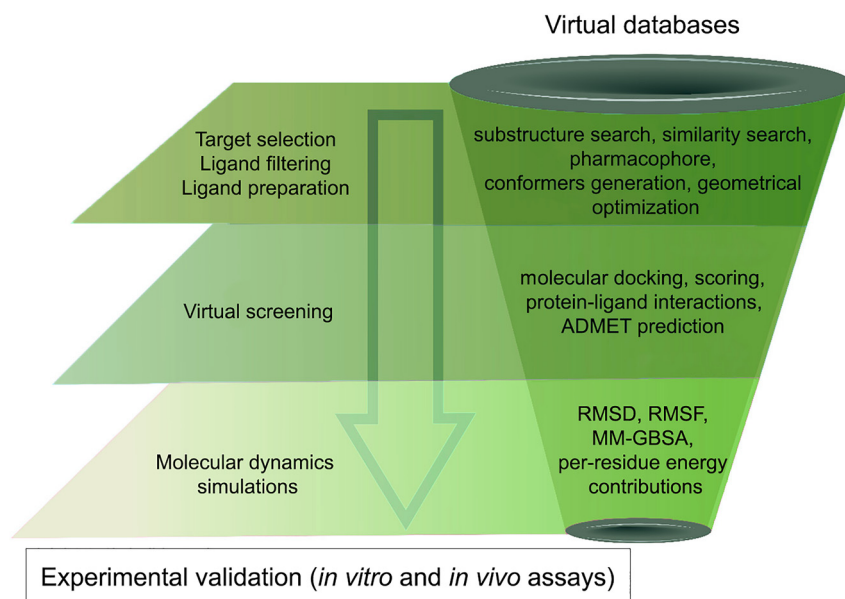


Figure 4: State-of-the-art virtual screening methodology to select and study natural products.

screens due to the presence of several disruptive functional groups that interact nonspecifically with various biological targets rather than selectively affecting the therapeutic target of interest [43]. Hepatotoxicity was predicted using the ProTox-II web server (https://tox-new.charite.de/prottox_II/) [44].

2.7 Molecular dynamics simulations

AMBER16 software [45] was employed to conduct molecular dynamics simulations on the most potent compounds in complex with MAO-B. AMBER force field 14SB [46] and the general AMBER force field (GAFF2) [47] were used to parametrize the protein and the identified inhibitors, respectively. The TIP3P water model with a margin of 15.0 Å (1.5 nm) in each direction from the solute was used to construct a water-solvated cubic box. The specifics of the used MD simulations are elucidated in Ref. [48–55]. In synopsis, energy minimization was initially used on the investigated inhibitors in complex with MAO-B for 5000 steps using the combined steepest and conjugate gradient algorithms. Thereafter, the minimized systems were progressively heated from 0 K to 300 K over 50 ps. The complexes were equilibrated to a free simulation for 1000 ps. Ultimately, a production run for 100 ns was subsequently carried out utilizing an NPT ensemble at 300 K with 1.0 atm pressure. All the periodic boundary PME (Particle Mesh Ewald) simulations were conducted using the “pmemd.cuda” implementation in AMBER for GPU-accelerated simulations on the CompChem hybrid GPU/CPU cluster.

2.8 MM-GBSA binding energy

The molecular mechanics-generalized Born surface area (MM-GBSA) approach was applied to estimate the binding free energies ($\Delta G_{\text{binding}}$) of the investigated inhibitors in complex with MAO-B [56]. Thus, the total binding free energies were evaluated according to IGB value of 2. For each system, the binding free energy calculations were executed for 10,000 snapshots recorded throughout 100 ns MD simulations. For each snapshot, the MM-GBSA ($\Delta G_{\text{binding}}$) binding energy was calculated by the standard formula:

$$\Delta G_{\text{binding}} = G_{\text{complex}} - (G_{\text{inhibitor}} + G_{\text{MAO-B}})$$

3 Results

Developing efficient therapies against neurodegenerative diseases such as Parkinson’s disease remains a great challenge. The use of natural products has been known for a long time to offer great promise and they’re often a safer alternative compared to synthesized drugs. Currently, *in silico* studies are providing much-needed preliminary data about potential drugs, which can be a great help in conducting additional *in vitro* and *in vivo* studies [57].

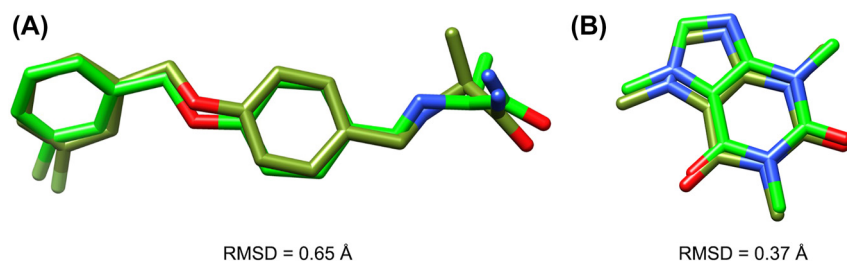


Figure 5: (A) Superposition and RMSD of crystal (green) and docked (olive green) structure of safinamide. (B) Superposition and RMSD of crystal (green) and docked (olive green) structure of caffeine.

3.1 Validation of molecular docking accuracy

Molecular docking protocol was first validated by cross-docking the co-crystallized ligands using the same parameters that were applied for the studied compounds against different crystallographic structures (PDB ID: 2V61 for MAO-B and PDB ID: 5IU4 for AA_{2A}R) [13, 58]. Computed root-mean-square deviation (RMSD) was calculated by mean of superposition; the obtained values are below 2 Å which indicates a good quality of the docking program (Figure 5).

Additionally, molecular docking accuracy was further validated using two datasets of 10 caffeine derivatives with reported half-maximal inhibitory concentrations (IC₅₀) for MAO-B and dissociation constants (K_i) for AA_{2A}R respectively [24, 59]. A good correlation was established between the docking results and the experimental values for MAO-B and AA_{2A}R, which confirms the reliability of the molecular docking approach to study the natural product-like caffeine derivatives with MAO-B. The correlation charts, correlation coefficients, and slopes are shown in Figure 6.

3.2 Natural product-like caffeine derivatives screening

In the present study, we screened 144 natural product-like caffeine derivatives against MAO-B using structure-based virtual screening. The compounds were ranked by their binding affinities (kcal/mol). The highest-ranking molecules displaying a docking score of -8.0 kcal/mol or less were further analyzed based on their interactions with the MAO-B active site cavity. Molecular docking results and protein-ligand interactions are shown in Table 1.

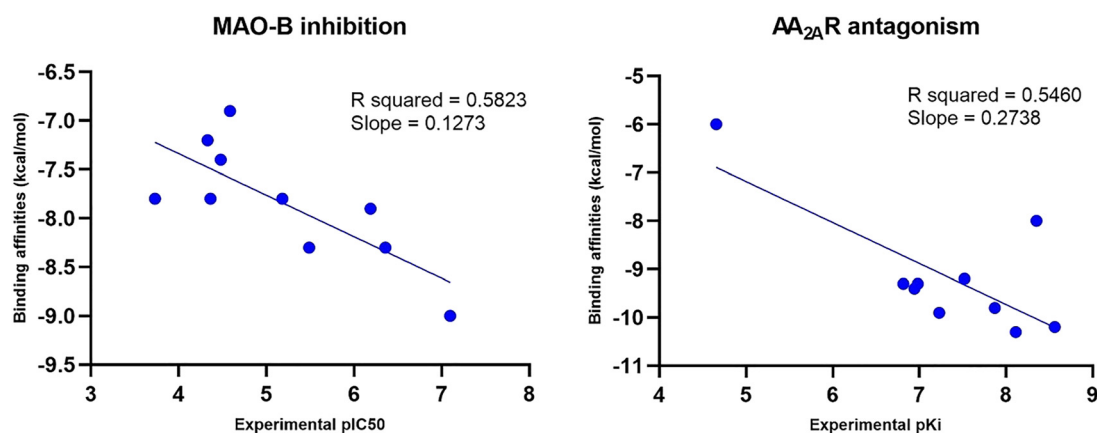


Figure 6: Correlation chart between molecular docking results and experimental pIC₅₀ for MAO-B (left) and experimental pK_i for AA_{2A}R (right).

Table 1: Docking results and protein-ligand interactions between the highest-scoring compounds and MAO-B.

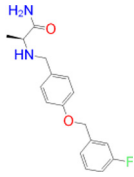
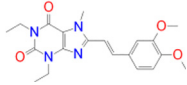
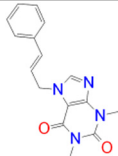
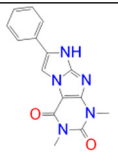
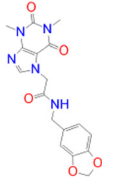
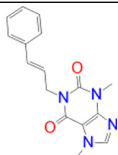
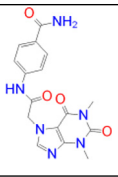
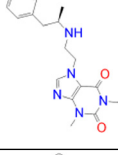
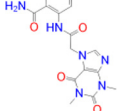
Compound	Chemical structure	Docking score (kcal/mol)	H bonds	Hydrophobic interactions
Safinamide		-9.9	GLN-206	TRP-119, TYR-60, LEU-164, LEU-171, TYR-326, PHE-168, GLN-206, TYR-398, TYR-435
Istradefylline		-9.3	FAD-1502	TYR-60, PRO-102, TYR-326, MET-341, LEU-328, GLN-206, ILE-199, TYR-398, TYR-435
CNP0202316		-10.1	CYS-172	TYR-60, LEU-328, TYR-326, PHE-343, TYR-398, ILE-316, LEU-171, ILE-198, ILE-199, CYS-172, PHE-168
CNP0298322		-9.8	ILE-199, TYR-435	PHE-168, ILE-164, ILE-316, ILE-198, CYS-172, TYR-398, TYR-60, PHE-343, LEU-328
CNP0369093		-9.8	CYS-172	ILE-199, LEU-171, ILE-199, ILE-316, TYR-326, FAD-1502, TYR-60, PHE-343
CNP0365210		-9.7	TYR-435	ILE-198, CYS-172, LEU-171, ILE-316, ILE-199, TYR-326, PHE-343, LEU-328, TYR-398
CNP0366822		-9.7	CYS-172	TYR-60, TYR-398, TYR-435, PHE-343, LEU-171, TYR-326, ILE-199, ILE-316, ILE-198
CNP0352436		-9.6	TYR-326	TYR-60, LEU-171, ILE-316, TYR-398, TYR-435, CYS-172, ILE-199
CNP0349562		-9.5	TYR-435, FAD-1502	ILE-199, ILE-316, LEU-171, PHE-168, TYR-326, LEU-328, PHE-343, TYR-60

Table 1: (continued).

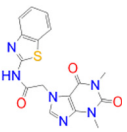
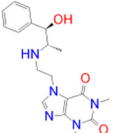
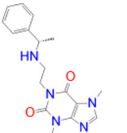
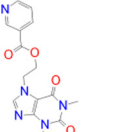
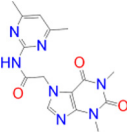
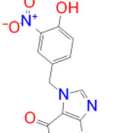
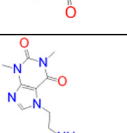
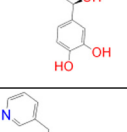
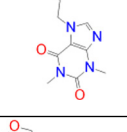
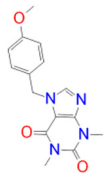
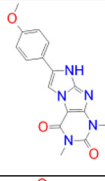
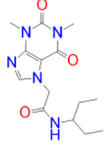
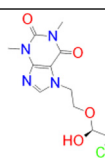
Compound	Chemical structure	Docking score (kcal/mol)	H bonds	Hydrophobic interactions
CNP0006822		-9.4	CYS-172, TYR-435, PRO-102, FAD-1502	TYR-60, PHE-343, LEU-328, LEU-171, ILE-199, TYR-398, GLN-206
CNP0074857		-9.2	GLN-206, LEU-171	TRP-119, LEU-167, TYR-398, TYR-326, ILE-199, ILE-316, PHE-168
CNP0390050		-9.1	GLN-206, TYR-435, LEU-171	TRP-119, ILE-199, ILE-316, CYS-172, PHE-343, TYR-60, TYR-398, PHE-168
CNP0089299		-9.0	GLN-206, TYR-435, FAD-1502	TYR-60, TYR-326, ILE-316, LEU-164, TRP-119, LEU-328, PHE-343, LEU-171, TYR-398
CNP0370968		-9.0	GLN-206, TYR-435, FAD-1502	PHE-343, TYR-60, TYR-326, ILE-316, LEU-164, LEU-328, LEU-171, CYS-172
CNP0338201		-8.9	ILE-198, TYR-435, FAD-1502	ILE-199, TYR-326, TYR-398, LEU-328, ILE-316, LEU-164, TYR-60, PHE-343, LEU-171
CNP0074614		-8.8	LEU-164, TYR-326, TYR-435, FAD-1502	ILE-198, TYR-398, LEU-171, TYR-60, PHE-343, LEU-328, CYS-172, ILE-199, ILE-316, LEU-167
CNP0212890		-8.7	ILE-199, FAD-1502	TYR-60, TYR-435, PHE-343, LEU-171, TYR-398, CYS-172, ILE-198
CNP0010096		-8.4	CYS-172	ILE-316, LEU-171, TYR-326, ILE-199, PHE-168, TYR-398, TYR-326, LEU-167

Table 1: (continued).

Compound	Chemical structure	Docking score (kcal/mol)	H bonds	Hydrophobic interactions
CNP0276217		-8.3	—	LEU-167, TYR-326, LEU-164, ILE-316, PRO-102, ILE-199, LEU-171, CYS-172, PHE-343, TYR-398
CNP0370378		-8.2	—	TRP-119, ILE-316, TYR-326, TYR-398, TYR-435, LEU-171, ILE-199, FAD-1502
CNP0224039		-8.2	TYR-435, FAD-1502	LEU-171, TYR-326, TYR-60, LEU-326, PHE-168
CNP0383986		-8.0	CYS-172	TYR-60, LEU-328, PHE-343, TYR-435, ILE-316

3.3 *In silico* ADMET prediction results

In silico pharmacokinetics, toxicity, and drug-likeness prediction results are shown in Table 2. All compounds were predicted as either soluble or highly soluble. Furthermore, most of the molecules are showing high gastro-intestinal absorption which indicates a good oral bioavailability. However, the blood-brain barrier permeability parameter revealed only two compounds besides safinamide that may readily cross the blood-brain barrier and act on the central nervous system. Moreover, all compounds, excluding safinamide, were identified as non-inhibitors of CYP2D6, which is particularly necessary for drugs acting on the brain since the expression of CYP2D6 is higher in the brain and is involved in metabolizing endogenous neural compounds that suggest its neuroprotective effects [60]. Moreover, the inhibition of CYP enzymes can decrease drug efficacy leading to therapeutic failure or increased drug side effects and toxicity [61–63]. Organ toxicity predicted using the ProTox-II webserver revealed that all the compounds are safe for the liver and do not disrupt its normal function. Physicochemical properties profiling of the selected compounds revealed that all the compounds are drug-like according to Lipinski's rule of five. Finally, Pain-assay interference compounds (PAINS) alerts calculations indicated that all the compounds do not contain any disruptive functional groups except CNP0074614 displaying one PAINS alert due to the catecholamine group.

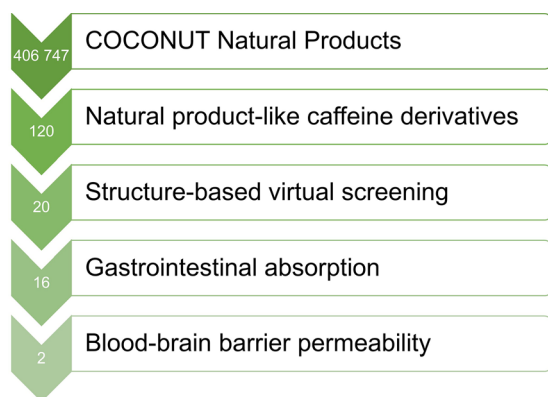
3.4 Interaction analysis of lead compounds with MAO-B and AA_{2A}R

According to the molecular docking and ADMET-based screening as summarized in Figure 7, two compounds were identified as potential drug candidates that possess the desired pharmacokinetics properties for drugs acting on the central nervous system: CNP0202316 and CNP0365210 superposed to the reference inhibitor, safinamide in complex with MAO-B are illustrated in Figure 8. The binding scores of these molecules were -10.1 and -9.7 kcal/mol for MAO-B respectively and are comparable to the reference inhibitor, safinamide

Table 2: Pharmacokinetics, toxicity prediction and drug likeness of the selected compounds.

Compound	Water solubility	GI absorption	BBB	CYP2D6 inhibitor	Hepatotoxicity	Lipinski violation	PAINS alert
Safinamide	-3.04	High	Yes	Yes	Inactive	0	0
Istradefylline	-3.83	High	No	No	Inactive	0	0
CNP0202316	-3.28	High	Yes	No	Inactive	0	0
CNP0298322	-3.67	High	No	No	Inactive	0	0
CNP0369093	-3.31	High	No	No	Inactive	0	0
CNP0365210	-3.28	High	Yes	No	Inactive	0	0
CNP0366822	-2.75	Low	No	No	Inactive	0	0
CNP0352436	-4.46	High	No	No	Inactive	0	0
CNP0349562	-2.75	Low	No	No	Inactive	0	0
CNP0006822	-3.72	High	No	No	Inactive	0	0
CNP0074857	-3.52	High	No	No	Inactive	0	0
CNP0390050	-4.07	High	No	No	Inactive	0	0
CNP0089299	-2.90	High	No	No	Inactive	0	0
CNP0370968	-3.20	High	No	No	Inactive	0	0
CNP0338201	-1.98	High	No	No	Inactive	0	0
CNP0074614	-2.33	Low	No	No	Inactive	0	1
CNP0212890	-3.67	High	No	No	Inactive	0	0
CNP0010096	-0.80	Low	No	No	Inactive	0	0
CNP0276217	-3.32	High	No	No	Inactive	0	0
CNP0370378	-3.79	High	No	No	Inactive	0	0
CNP0224039	-2.30	High	No	No	Inactive	0	0
CNP0383986	-2.15	High	No	No	Inactive	0	0

Water solubility, insoluble < -10 < poorly < -6 < moderately < -4 < soluble < -2 < very < 0 < highly; **GI absorption**, gastrointestinal absorption; **BBB**, blood-brain barrier permeability; **CYP2D6 inhibitor**, Likelihood of a drug to act as inhibitor of cytochrome P450 CYP2D6; **Hepatotoxicity**, prediction of drug-induced liver injury; **Lipinski violation**, number of violations to the rule of five ($\log P_{o/w} \leq 5$; MW ≤ 500 g/mol; HBA ≤ 10 ; HBD ≤ 5 ; RB ≤ 10); **PAINS alert**, number of disruptive functional groups shared by many PAINS (Pan-assay interference compounds).

**Figure 7:** Step-wise structure and ADMET-based screening of the selected natural product-like caffeine derivatives.

which displayed a binding score of -9.9 kcal/mol. However, molecular docking of istradefylline revealed a low binding affinity (-9.3 kcal/mol) compared to the aforementioned compounds.

Safinamide was found to interact through hydrogen bonding with GLN-206 which is known to be a hydrogen bond acceptor for the majority of MAO-B inhibitors and is by the literature [13]. Structural analysis shows that both compounds share a phenyl ring linked to the caffeine scaffold with a pentane group. The phenyl ring seems to be favorable for the stability of the ligands within the MAO-B active site by establishing numerous hydrophobic interactions with the nearby residues of the entrance cavity. Meanwhile, the caffeine

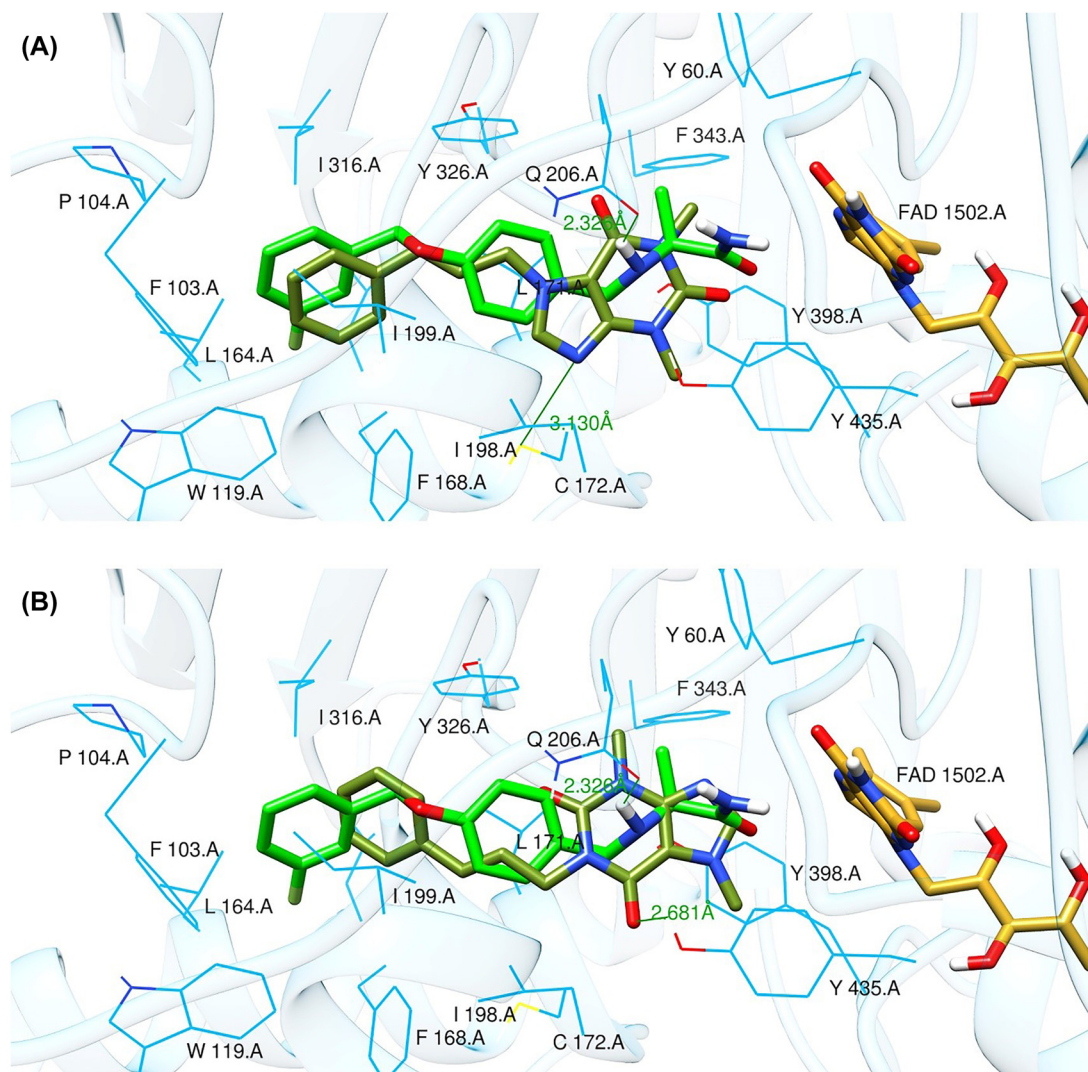


Figure 8: Binding poses of selected lead compounds: CNP0202316 (A) and CNP0365210 (B) (shown in olive green color) with MAO-B and superposed to safinamide (shown in green color).

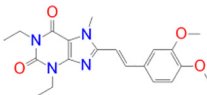
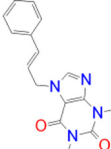
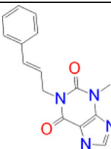
scaffold is directed towards the FAD cofactor and interacts with CYS-172 in CNP0202316 and TYR-435 of the aromatic cage in CNP0365210 through hydrogen bonding.

It has been shown in previous studies that hydrophobic interactions through the phenyl ring are vital for establishing MAO-B binding and are more favorable than all other interactions such as hydrogen or halogen bonds [64]. However, CNP0202316 where the phenyl ring is placed at C7 of the xanthine core seems to be more stable than the second compound implying that the presence of hydrophilic interaction with CYS-172 contributes more to the anchoring and the stability of this compound in the active site cavity of MAO-B.

Alternatively, the selected compounds were analyzed through molecular docking studies with AA_{2A}R to assess their binding affinities with the AA_{2A}R active site and compare their binding conformations to istradefylline. Molecular docking results and protein-ligand interactions are shown in Table 3.

The binding poses of the selected compounds and istradefylline were superposed to the co-crystallized structure of caffeine (Figure 9). The structural analysis indicates that both compounds were able to interact with a key polar residue, ASN-253 through the formation of hydrophilic hydrogen bonds, similarly to istradefylline and other potent AA_{2A}R antagonists [65]. A large network of hydrophobic interactions was also

Table 3: Molecular docking results and protein-ligand interactions of selected lead compounds with AA_{2A}R.

Compound	Chemical structure	Docking score (kcal/mol)	H bonds	Hydrophobic interactions
Istradefylline		-8.0	ASN-253	ALA-81, PHE-168, GLU-169, MET-174, LEU-249, TYR-271
CNP0202316		-8.7	ASN-253	LEU-85, ILE-66, LEU-167, PHE-168, GLU-169, TRP-246, LEU-249, ILE-274, LEU-267, TYR-271
CNP0365210		-8.0	ASN-253	LEU-85, ILE-66, PHE-168, GLU-169, TRP-246, LEU-267, TYR-271

observed, where key residues namely PHE-168 and GLU-169 were found to make a consistent appearance. Since all compounds share the same core that characterizes the caffeine molecule, this would entail a somewhat similar disposition inside the binding pocket. This holds especially for CNP0202316 where the xanthine core was found to be positioned similarly to istradefylline. Moreover, the propylbenzene moiety at position C7 in CNP0202316 might be more favorable to the hydrophobic pocket of the receptor suggesting its affinity potential which may be on par or better than istradefylline.

3.5 Molecular dynamics simulations and binding energy calculations

Molecular dynamics (MD) simulations were applied to probe the stability of the selected ligand-protein complexes, structural specifics, conformational flexibilities, and realize reliable inhibitor-enzyme binding affinities [66, 67]. The most promising compounds in complex with the MAO-B enzyme were further inspected via MD throughout 100 ns simulation time. According to the gathered inhibitor-enzyme snapshots over the production run of 100 ns, the MM-GBSA approach was used to calculate the binding free energies ($\Delta G_{\text{binding}}$) and are illustrated in Figure 10. From the data in Figure 10, it is apparent that the CNP0202316 and CNP0365210 demonstrated auspicious binding affinities with values of -36.7 and -34.5 kcal/mol, respectively, and are comparable to the reference inhibitor, safinamide ($\Delta G_{\text{binding}} = -37.9$ kcal/mol). The comparison of safinamide with CNP0202316 and CNP0365210 unveiled competing for binding affinities proposing the *in silico* prospectivity of the two molecules as MAO-B inhibitors.

The calculated MM-GBSA binding energies were then decomposed into separate components to recognize the vigor in the binding of MAO-B with CNP0202316, CNP0365210, and safinamide (Figure 10). The van der Waals (ΔE_{vdw}) energy was a considerable contributor to CNP0202316, CNP0365210, and safinamide-MAO-B binding affinities with average values of -50.9 , -46.8 , and -47.3 kcal/mol, respectively. ΔE_{ele} was effectual with average values of -5.2 , -11.1 , and -25.3 kcal/mol for the CNP0202316, CNP0365210, and safinamide-MAO-B binding affinities, respectively.

The binding energies of CNP0202316, CNP0365210, and safinamide in complex with MAO-B were further decomposed at the per-residue level, and the amino acid residues with free energy contribution < -0.50 kcal/mol were depicted (Figure 11). LEU-171, GLN-206, and TYR-326 in the MAO-B complex appropriately share with CNP0202316, CNP0365210, and safinamide. There was significant participation by LEU-171 to the

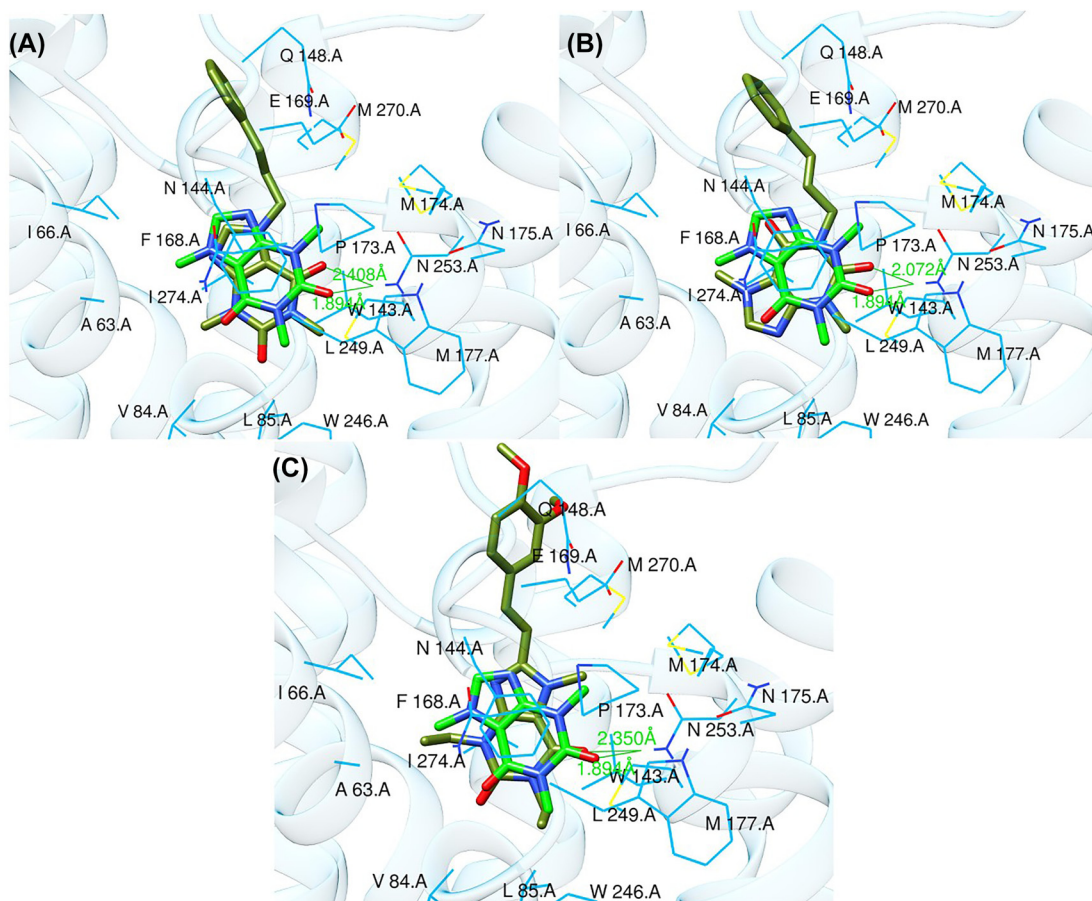


Figure 9: Binding poses of CNP0202316 (A), CNP0365210 (B), and istradefylline (C) (shown in olive green color) with $AA_{2A}R$ and superposed to the crystal structure of caffeine (shown in green color).

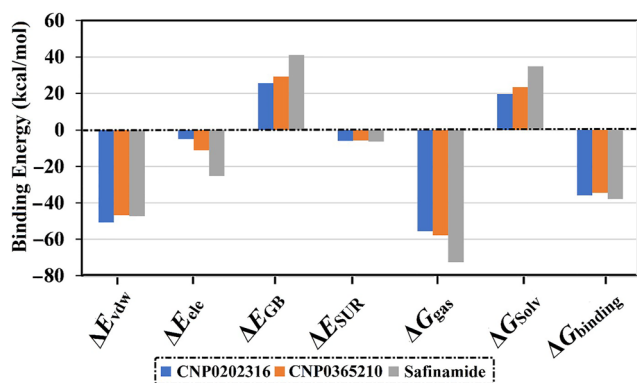


Figure 10: Decomposition of MM-GBSA binding energies for the investigated inhibitors in complex with MAO-B throughout 100 ns MD simulations.

total binding free energy with values of -2.0 , -3.0 , and -2.2 kcal/mol for CNP0202316-, CNP0365210- and safinamide-MAO-B complexes, respectively.

3.6 Post-MD simulations analysis

Molecular docking calculations, and MD simulations combined with MM-GBSA binding energy calculations, unveiled the most potent molecules as potential MAO-B inhibitors. The MD-based analysis could be required

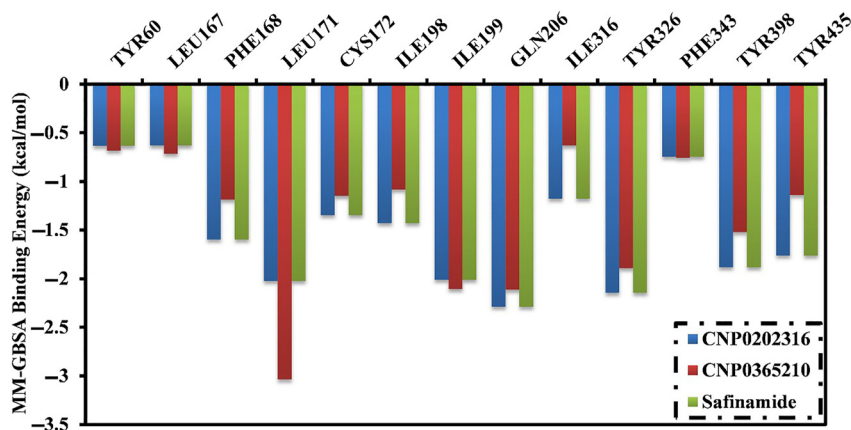


Figure 11: Energy contributions (kcal/mol) for MAO-B amino acid residues to the binding free energy of CNP0202316, CNP0365210, and safinamide.

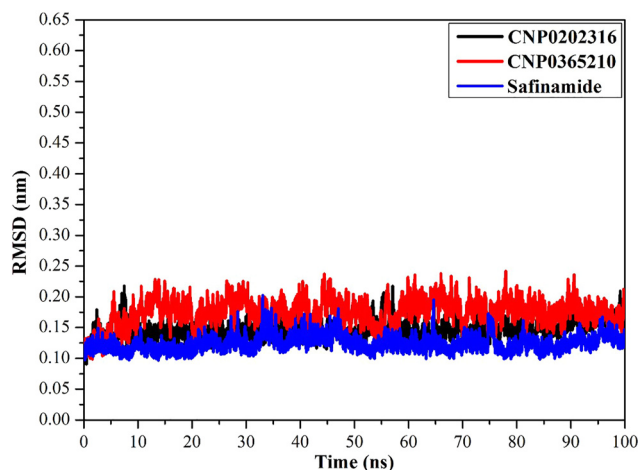


Figure 12: Root-mean-square deviation (RMSD) of the backbone atoms from the starting structure of CNP0202316 (in black), CNP0365210 (in red), and safinamide (in blue) with MAO-B during the 100 ns MD simulations.

to demonstrate structural and energetic stabilities for the scrutinized inhibitors in complex with MAO-B. The structural and energetical analysis included root-mean-square deviation (RMSD), Center-of-Mass (CoM) distance, and binding energy per-frame.

3.6.1 Root-mean-square deviation (RMSD)

The root-mean-square deviation (RMSD) values of the backbone atoms within the whole complex throughout the simulation time were estimated to monitor the structural stability of the CNP0202316, CNP0365210, and safinamide in complex with MAO-B. The RMSD of the backbone atoms as a function of time following the initial structure of the three investigated systems is displayed in Figure 12. The platform in RMSD curves emphasizes that all three inspected systems attain an equilibrium within 1000–10,000 ps throughout MD simulations, exposing that the three investigated systems are converged over the simulation window. These findings suggest that all the compounds are tightly bound and not influenced by the topology of the protein. This is especially true for CNP0202316, which displayed very slight deviations somewhat similar to safinamide suggesting its high stability compared to CNP0365210.

3.6.2 Center-of-mass distance

To get a more in-depth insight into the stability of the selected compounds throughout the MD simulation time, center-of-mass (CoM) distances were evaluated (Figure 13). The most interesting aspect of this graph is

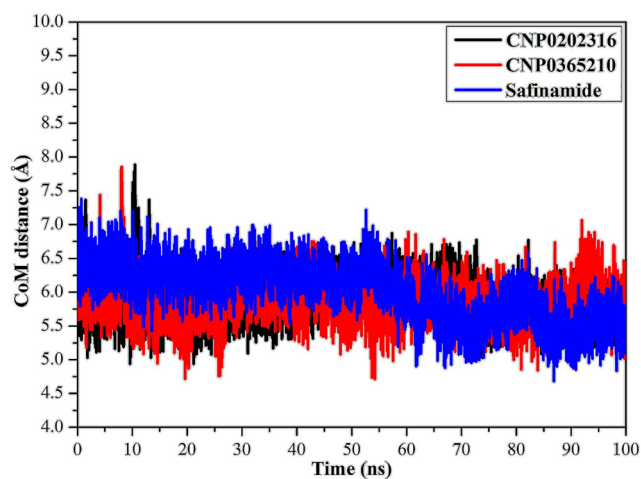


Figure 13: Center-of-mass (CoM) distances (in Å) between CNP0202316 (in black), CNP0365210 (in red), and safinamide (in blue) and TYR324 of MAO-B throughout a 100 ns MD simulation.

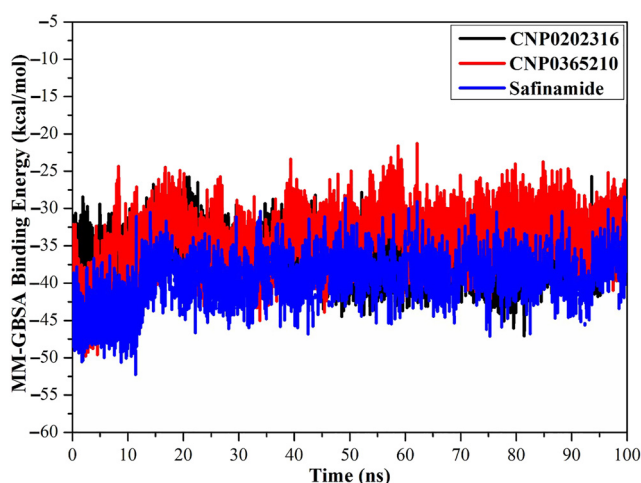


Figure 14: Estimated MM-GBSA binding energy per frame for CNP0202316 (in black), CNP0365210 (in red), and safinamide (in blue) with MAO-B over a 100 ns MD simulation.

that CoM distances were consistent for the CNP0202316- and CNP0365210 in complex with MAO-B compared to safinamide-MAO-B complex, with average values of 5.7, 5.8, and 6.1 Å, respectively. The most obvious finding to emerge from this analysis is that CNP0202316 and CNP0365210 bound more tightly to the MAO-B complex than the reference inhibitor, safinamide.

3.6.3 Binding energy per frame

The comprehensive structural stability of CNP0202316, CNP0365210, and safinamide complexed with MAO-B was evaluated throughout a 100 ns MD simulation via inspecting the correlation between the binding energy per frame and time (Figure 14). Overall stabilities for CNP0202316, CNP0365210, and safinamide were noticed with average binding energies ($\Delta G_{\text{binding}}$) of -36.6 , -34.5 , and -37.9 kcal/mol, respectively. Based on this analysis, all investigated complexes preserved their stability over the 100 ns MD simulations.

4 Discussion

The results obtained from the molecular docking study with MAO-B were further analyzed through molecular dynamics simulations and binding free energy calculations. MM-GBSA binding energies further confirmed that van der Waals (ΔE_{vdw}) energy is a considerable contributor to the stability of MAO-B inhibitors. This

finding confirms that hydrophobic interactions outweigh any other interactions in terms of MAO-B inhibition, and is also supported by the literature [65]. Post-MD simulations analysis confirmed the stability of the three compounds and revealed that all the complexes achieve equilibrium within 1–10 ns throughout the simulation time. These results suggest that the proposed natural products may be on par or better than the inhibitor of reference, safinamide regarding MAO-B inhibition. The key residues involved in MAO-B inhibition were found to be LEU-171, ILE-199, TYR-326, and GLN-206, these residues contribute the most to the stability of the inhibitors when bound to MAO-B. LEU-171, ILE-199, and TYR-326 are specific residues to MAO-B isoform, they are located in the entrance cavity and play a role in substrate and inhibitor specificity [68, 69]. Meanwhile, GLN-206 is recognized as a hydrogen bond acceptor for most MAO-B inhibitors and is responsible for their stability in the substrate cavity [17]. Moreover, the identified compounds may confer neuroprotective properties linked to the xanthine core as reported in the literature [70]. For MAO-B, the orientation of the phenyl ring linked to the xanthine core was found to be similar to safinamide especially in CNP0202316, and is favorable to the entrance hydrophobic cavity. On the other hand, this molecule adopted a similar conformation to istradefylline when bound to AA_{2A}R. The propylbenzene moiety attached to the imidazole of the caffeine in CNP0202316 at position C7 is more favorable to the hydrophobic pocket of AA_{2A}R, whereas the oxygen atom of the xanthine core maintained a hydrogen bond with ASN-253 that is deemed crucial to the binding of most AA_{2A}R antagonists [71]. Thus, the identified compounds might offer a dual-target activity in the context of a polypharmacological approach and might represent a more efficient alternative for treating and slowing down the neuronal damage in Parkinson's disease patients.

5 Conclusions

The present study aimed to find novel natural product-like caffeine derivatives as potential dual MAO-B inhibitors/AA_{2A}R antagonists. Structure-based virtual screening and ADMET analysis revealed two natural products that fulfill the requirements for drugs acting on the brain. The selected compounds in complex with MAO-B were subject to molecular dynamics simulations to assess their stability over the simulation time along with the inhibitor of reference, safinamide. Our findings show that the presence of the phenyl ring in the selected compounds is crucial for the ligands to fill the long-shaped cavity of the MAO-B active site and is a major contributor to various van der Waals interactions responsible for the stability and the tight-binding of these compounds to MAO-B. Similarly, the propylbenzene moiety was found to be more favorable for the hydrophobic pocket of AA_{2A}R especially when linked at position C7 of the xanthine core which allowed the caffeine core to adopt a similar conformation to istradefylline suggesting the dual-target properties of the identified natural products. In conclusion, the structure-based virtual screening helped provide valuable insight on the studied natural product-like caffeine derivatives and our findings may attract more focus for the development of novel antiparkinsonian drugs with dual-targeting properties. However, *in vitro* experiments such as bioactivity assays for MAO-B and AA_{2A}R, membrane permeability and cell viability assays remains necessary to further validate these findings.

Acknowledgments: We would like to thank Prof. Phillip E. Barnes, University of South Carolina, Columbia, for proofreading the manuscript, and Prof. Francisco Javier Luque Garriga, University of Barcelona, Spain, for his constructive criticism. Their contribution is sincerely appreciated and gratefully acknowledged.

Author contribution: All the authors have accepted responsibility for the entire content of this submitted manuscript and approved submission.

Research funding: The computational work was completed with resources supported by the Science and Technology Development Fund, STDF, Egypt, Grants No. 5480 & 7972 (Granted to Dr. Mahmoud A. A. Ibrahim).

Conflict of interest statement: The authors declare that they have no conflict of interest.

Ethical Approval: This article does not contain any studies with animals performed by any of the authors.

References

1. Barnham KJ, Masters CL, Bush AI. Neurodegenerative diseases and oxidative stress. *Nat Rev Drug Discov* 2004;3:205–14.
2. Moya-Alvarado G, Gershoni-Emek N, Perlson E, Bronfman FC. Neurodegeneration and Alzheimer's disease (AD). What can proteomics tell us about the Alzheimer's brain? *Mol Cell Proteomics* 2016;15:409–25.
3. Noda S, Sato S, Fukuda T, Tada N, Uchiyama Y, Tanaka K, et al. Loss of Parkin contributes to mitochondrial turnover and dopaminergic neuronal loss in aged mice. *Neurobiol Dis* 2020;136:104717.
4. Davie CA. A review of Parkinson's disease. *Br Med Bull* 2008;86:109–27.
5. Youdim MB, Edmondson D, Tipton KF. The therapeutic potential of monoamine oxidase inhibitors. *Nat Rev Neurosci* 2006;7:295–309.
6. Hickey P, Stacy M. Adenosine A2A antagonists in Parkinson's disease: what's next? *Curr Neurol Neurosci Rep* 2012;12:376–85.
7. Shih JC, Chen K, Ridd MJ. Monoamine oxidase: from genes to behavior. *Annu Rev Neurosci* 1999;22:197–217.
8. Culpepper L. Reducing the burden of difficult-to-treat major depressive disorder: revisiting monoamine oxidase inhibitor therapy. *Prim Care Companion CNS Diso* 2013;15:27220.
9. Tetrad JW, Koller WC. A novel formulation of selegiline for the treatment of Parkinson's disease. *Neurology* 2004;63(7 Suppl 2):S2–6.
10. Finberg JP, Rabey JM. Inhibitors of MAO-A and MAO-B in psychiatry and neurology. *Front Pharmacol* 2016;7:340.
11. Mallajosyula JK, Kaur D, Chinta SJ, Rajagopalan S, Rane A, Nicholls DG, et al. MAO-B elevation in mouse brain astrocytes results in Parkinson's pathology. *PLoS One* 2008;3:e1616.
12. Youdim MB, Gross A, Finberg JP. Rasagiline [N-propargyl-1R (+)-aminoindan], a selective and potent inhibitor of mitochondrial monoamine oxidase B. *Br J Pharmacol* 2001;132:500–6.
13. Binda C, Wang J, Pisani L, Caccia C, Carotti A, Salvati P, et al. Structures of human monoamine oxidase B complexes with selective noncovalent inhibitors: safinamide and coumarin analogs. *J Med Chem* 2007;50:5848–52.
14. Dungo R, Deeks ED. Istradefylline: first global approval. *Drugs* 2013;73:875–82.
15. Chen JF, Cunha RA. The belated US FDA approval of the adenosine A2A receptor antagonist istradefylline for treatment of Parkinson's disease. *Purinergic Signal* 2020;16:167–74.
16. Preti D, Baraldi PG, Moorman AR, Borea PA, Varani K. History and perspectives of A2A adenosine receptor antagonists as potential therapeutic agents. *Med Res Rev* 2015;35:790–848.
17. Binda C, Li M, Hubálek F, Restelli N, Edmondson DE, Mattevi A. Insights into the mode of inhibition of human mitochondrial monoamine oxidase B from high-resolution crystal structures. *Proc Natl Acad Sci USA* 2003;100:9750–5.
18. Mostert S, Petzer A, Petzer JP. Indanones as high-potency reversible inhibitors of monoamine oxidase. *ChemMedChem* 2015;10:862–73.
19. Edmondson DE, Binda C, Mattevi A. Structural insights into the mechanism of amine oxidation by monoamine oxidases A and B. *Arch Biochem Biophys* 2007;464:269–76.
20. Binda C, Newton-Vinson P, Hubálek F, Edmondson DE, Mattevi A. Structure of human monoamine oxidase B, a drug target for the treatment of neurological disorders. *Nat Struct Biol* 2002;9:22–6.
21. Carradori S, D'Ascenzio M, Chimenti P, Secci D, Bolasco A. Selective MAO-B inhibitors: a lesson from natural products. *Mol Divers* 2014;18:219–43.
22. Khanam S, Subitsha AJ, Sabu S. Plants as a promising source for the treatment of parkinson disease: a systemic review. *IP Int J Compr Adv Pharmacol* 2021;5:158–66.
23. Pitsillou E, Liang J, Karagiannis C, Ververis K, Darmawan KK, Ng K, et al. Interaction of small molecules with the SARS-CoV-2 main protease in silico and in vitro validation of potential lead compounds using an enzyme-linked immunosorbent assay. *Comput Biol Chem* 2020;89:107408.
24. Pretorius J, Malan SF, Castagnoli N Jr, Bergh JJ, Petzer JP. Dual inhibition of monoamine oxidase B and antagonism of the adenosine A2A receptor by (E, E)-8-(4-phenylbutadien-1-yl) caffeine analogues. *Bioorg Med Chem* 2008;16:8676–84.
25. Azam F, Madi AM, Ali HI. Molecular docking and prediction of pharmacokinetic properties of dual mechanism drugs that block MAO-B and adenosine A2A receptors for the treatment of Parkinson's disease. *J Young Pharm* 2012;4:184–92.
26. Petzer A, Pienaar A, Petzer JP. The interactions of caffeine with monoamine oxidase. *Life Sci* 2013;93:283–7.
27. Mathur R, Velpandian T. Medicinal plant-based health products: where is the medicinal constituent? *Indian J Pharmacol* 2009;41:205.
28. Essa MM, Braidy N, Bridge W, Subash S, Manivasagam T, Vijayan RK, et al. Review of natural products on Parkinson's disease pathology. *J Aging Res Clin Pract* 2014;3:1–8.
29. Fisone G, Borgkvist A, Usiello A. Caffeine as a psychomotor stimulant: mechanism of action. *Cell Mol Life Sci CMLS* 2004;61:857–72.
30. Sorokina M, Merseburger P, Rajan K, Yirik MA, Steinbeck C. COCONUT online: collection of open natural products database. *J Cheminf* 2021;13:1–3.

31. Agrafiotis DK, Lobanov VS, Shemanarev M, Rassokhin DN, Izrailev S, Jaeger EP, et al. Efficient substructure searching of large chemical libraries: the ABCD chemical cartridge. *J Chem Inf Model* 2011;51:3113–30.
32. Jo S, Kim T, Iyer VG, Im W. CHARMM-GUI: a web-based graphical user interface for CHARMM. *J Comput Chem* 2008;29:1859–65.
33. Boulaamane Y, Ahmad I, Patel H, Das N, Britel MR, Maurady A. Structural exploration of selected C6 and C7-substituted coumarin isomers as selective MAO-B inhibitors. *J Biomol Struct Dyn* 2022;24:1–5.
34. Morris GM, Huey R, Lindstrom W, Sanner MF, Belew RK, Goodsell DS, et al. AutoDock4 and AutoDockTools4: automated docking with selective receptor flexibility. *J Comput Chem* 2009;30:2785–91.
35. O’Boyle NM, Banck M, James CA, Morley C, Vandermeersch T, Hutchison GR. Open Babel: an open chemical toolbox. *J Cheminf* 2011;3:1–4.
36. Trott O, Olson AJ. AutoDock Vina: improving the speed and accuracy of docking with a new scoring function, efficient optimization, and multithreading. *J Comput Chem* 2010;31:455–61.
37. Santana K, do Nascimento LD, Lima e Lima A, Damasceno V, Nahum C, Braga RC, et al. Applications of virtual screening in bioprospecting: facts, shifts, and perspectives to explore the chemo-structural diversity of natural products. *Front Chem* 2021;9:155.
38. Pettersen EF, Goddard TD, Huang CC, Couch GS, Greenblatt DM, Meng EC, et al. UCSF Chimera—a visualization system for exploratory research and analysis. *J Comput Chem* 2004;25:1605–12.
39. Biovia DS. Discovery studio visualizer. San Diego, CA, USA: Dassault Systèmes; 2017:936 p.
40. Kar S, Leszczynski J. Open access in silico tools to predict the ADMET profiling of drug candidates. *Expet Opin Drug Discov* 2020;15:1473–87.
41. Daina A, Michielin O, Zoete V. SwissADME: a free web tool to evaluate pharmacokinetics, drug-likeness and medicinal chemistry friendliness of small molecules. *Sci Rep* 2017;7:1–3.
42. Lipinski CA. Lead-and drug-like compounds: the rule-of-five revolution. *Drug Discov Today Technol* 2004;1:337–41.
43. Baell JB. Feeling nature’s PAINS: natural products, natural product drugs, and pan assay interference compounds (PAINS). *J Nat Prod* 2016;79:616–28.
44. Banerjee P, Eckert AO, Schrey AK, Preissner R. ProTox-II: a webserver for the prediction of toxicity of chemicals. *Nucleic Acids Res* 2018;46:W257–63.
45. Case DA, Betz RM, Cerutti DS, Cheatham T, Darden T, Duke RE, et al. Amber 16, University of California, San Francisco. San Francisco: University of California; 2016.
46. Maier JA, Martinez C, Kasavajhala K, Wickstrom L, Hauser KE, Simmerling C. ff14SB: improving the accuracy of protein side chain and backbone parameters from ff99SB. *J Chem Theor Comput* 2015;11:3696–713.
47. Wang J, Wolf RM, Caldwell JW, Kollman PA, Case DA. Development and testing of a general amber force field. *J Comput Chem* 2004;25:1157–74.
48. Ibrahim MA, Abdelrahman AH, Hassan AM. Identification of novel Plasmodium falciparum PI4KB inhibitors as potential anti-malarial drugs: homology modeling, molecular docking and molecular dynamics simulations. *Comput Biol Chem* 2019;80:79–89.
49. Ibrahim MA, Abdeljawaad KA, Abdelrahman AH, Hegazy ME. Natural-like products as potential SARS-CoV-2 Mpro inhibitors: in-silico drug discovery. *J Biomol Struct Dyn* 2020;39:5722–34.
50. Ibrahim MA, Abdelrahman AH, Hegazy ME. In-silico drug repurposing and molecular dynamics puzzled out potential SARS-CoV-2 main protease inhibitors. *J Biomol Struct Dyn* 2021;39:5756–67.
51. Ibrahim MA, Abdelrahman AH, Hussien TA, Badr EA, Mohamed TA, El-Seedi HR, et al. In silico drug discovery of major metabolites from spices as SARS-CoV-2 main protease inhibitors. *Comput Biol Med* 2020;126:104046.
52. Ibrahim MA, Abdelrahman AH, Allemailem KS, Almatroudi A, Moustafa MF, Hegazy ME. In silico evaluation of prospective anti-COVID-19 drug candidates as potential SARS-CoV-2 main protease inhibitors. *Protein J* 2021;40:296–309.
53. Ibrahim MA, Abdelrahman AH, Mohamed TA, Atia MA, Al-Hammady MA, Abdeljawaad KA, et al. In silico mining of terpenes from red-sea invertebrates for SARS-CoV-2 main protease (Mpro) inhibitors. *Molecules* 2021;26:2082.
54. Ibrahim MA, Badr EA, Abdelrahman AH, Almansour NM, Shawky AM, Mekhemer GA, et al. Prospective drug candidates as human multidrug transporter ABCG2 inhibitors: an in silico drug discovery study. *Cell Biochem Biophys* 2021;79:189–200.
55. Ibrahim MA, Mohamed EA, Abdelrahman AH, Allemailem KS, Moustafa MF, Shawky AM, et al. Rutin and flavone analogs as prospective SARS-CoV-2 main protease inhibitors: in silico drug discovery study. *J Mol Graph Model* 2021;105:107904.
56. Massova I, Kollman PA. Combined molecular mechanical and continuum solvent approach (MM-PBSA/GBSA) to predict ligand binding. *Perspect Drug Discov Des* 2000;18:113–35.
57. Singh R, Gautam A, Chandel S, Ghosh A, Dey D, Roy S, et al. Protease inhibitory effect of natural polyphenolic compounds on SARS-CoV-2: an in silico study. *Molecules* 2020;25:4604.
58. Segala E, Guo D, Cheng RK, Bortolato A, Deflorian F, Dore AS, et al. Controlling the dissociation of ligands from the adenosine A2A receptor through modulation of salt bridge strength. *J Med Chem* 2016;59:6470–9.

59. Petzer A, Grobler P, Bergh JJ, Petzer JP. Inhibition of monoamine oxidase by selected phenylalkylcaffeine analogues. *J Pharm Pharmacol* 2014;66:677–87.
60. Da Prada M, Zürcher G, Wüthrich I, Haefely WE. On tyramine, food, beverages and the reversible MAO inhibitor moclobemide. *J Neural Transm Suppl* 1988;26:31–56.
61. Guengerich FP. Cytochrome p450 and chemical toxicology. *Chem Res Toxicol* 2008;21:70–83.
62. Lin JH, Lu AY. Inhibition and induction of cytochrome P450 and the clinical implications. *Clin Pharmacokinet* 1998;35:361–90.
63. Pelkonen O, Turpeinen M, Hakkola J, Honkakoski P, Hukkanen J, Raunio H. Inhibition and induction of human cytochrome P450 enzymes: current status. *Arch Toxicol* 2008;82:667–715.
64. Rauhamäki S, Postila PA, Niinivehmas S, Kortet S, Schildt E, Pasanen M, et al. Structure-activity relationship analysis of 3-phenylcoumarin-based monoamine oxidase B inhibitors. *Front Chem* 2018;6:41.
65. de Lera Ruiz M, Lim YH, Zheng J. Adenosine A2A receptor as a drug discovery target. *J Med Chem* 2014;57:3623–50.
66. De Vivo M, Masetti M, Bottegoni G, Cavalli A. Role of molecular dynamics and related methods in drug discovery. *J Med Chem* 2016;59:4035–61.
67. Kerrigan JE. Molecular dynamics simulations in drug design. In: Kortagere S, editors. *In silico models for drug discovery*. Totowa, NJ: Humana Press; 2013; vol. 993: 95–113 pp.
68. Geha RM, Rebrin I, Chen K, Shih JC. Substrate and inhibitor specificities for human monoamine oxidase A and B are influenced by a single amino acid. *J Biol Chem* 2001;276:9877–82.
69. Milczek EM, Binda C, Rovida S, Mattevi A, Edmondson DE. The ‘gating’ residues Ile199 and Tyr326 in human monoamine oxidase B function in substrate and inhibitor recognition. *FEBS J* 2011;278:4860–9.
70. Kasabova-Angelova A, Tzankova D, Mitkov J, Georgieva M, Tzankova V, Zlatkov A, et al. Xanthine derivatives as agents affecting non-dopaminergic neuroprotection in Parkinson’s disease. *Curr Med Chem* 2020;27:2021–36.
71. Jaakola VP, Lane JR, Lin JY, Katritch V, Iljerman AP, Stevens RC. Ligand binding and subtype selectivity of the human A2A adenosine receptor: identification and characterization of essential amino acid residues. *J Biol Chem* 2010;285:13032–44.